Determination of the Gas-Phase Acidities of Cysteine-Polyalanine Peptides Using the Extended Kinetic Method

John P. Tan and Jianhua Ren

Department of Chemistry, University of the Pacific, Stockton, California, USA

We determined the gas-phase acidities of two cysteine-polyalanine peptides, $HSCA_3$ and $HSCA_4$, using a triple-quadrupole mass spectrometer through application of the extended kinetic method with full entropy analysis. Five halogenated carboxylic acids were used as the reference acids. The negatively charged proton-bound dimers of the deprotonated peptides with the conjugate bases of the reference acids were generated by electrospray ionization. Collision-induced dissociation (CID) experiments were carried out at three collision energies. The enthalpies of deprotonation ($\Delta_{acid}H$) of the peptides were derived according to the linear relationship between the logarithms of the CID product ion branching ratios and the differences of the gas-phase acidities. The values were determined to be $\Delta_{acid}H(HSCA_3) =$ 317.3 ± 2.4 kcal/mol and $\Delta_{acid}H (HSCA_4)$ = 316.2 ± 3.9 kcal/mol. Large entropy effects ($\Delta(\Delta S)$ = 13–16 cal/mol K) were observed for these systems. Combining the enthalpies of deprotonation with the entropy term yielded the apparent gas-phase acidities ($\Delta_{acid}G^{app}$) of 322.1 ± 2.4 kcal/mol ($HSCA_3$) and 320.1 ± 3.9 kcal/mol ($HSCA_4$), in agreement with the results obtained from the CID-bracketing experiments. Compared with that in the isolated cysteine residue, the thiol group in $HSCA_{3,4}$ has a stronger gas-phase acidity by about 20 kcal/mol. This increased acidity is likely due to the stabilization of the negatively charged thiolate group through internal solvation.   (J Am Soc Mass Spectrom 2007, 18, 188–194) © 2007 American Society for Mass Spectrometry

In connection with the investigations of the unusual acidities of the cysteine residue at the active sites of the thioredoxin family of enzymes, we have studied a series of cysteine-polyalanine peptides. One of the important functions of the thioredoxin family of enzymes is to catalyze the reduction of the disulfide bonds in proteins, an important step involved in protein folding/unfolding processes [1]. The measured pK_a values of the thiol group (SH) of the active site cysteine residue range from 3.5 to 6.7, significantly lower than those in unfolded proteins or an isolated cysteine (pK_a ~ 8.5) [2, 3]. The nature of the unusually acidic cysteine is unclear. Although extensive studies have been carried out in aqueous solutions, the interpretation of the results was complicated because of solvent effects [4]. Gas-phase studies with carefully designed model molecules can provide valuable information in understanding the factors influencing the acidity of the active-site cysteine residue in these enzymes. We have designed a series of peptides, including cysteine-polyalanines, which could mimic the conformation of the active site in thioredoxin. At the current stage, we are developing

methodologies that could be used to measure the acidities of these peptides. In particular, we apply the extended Cooks' kinetic method [5–7]. An important issue involved in the experimental measurements is the entropy effect associated with the conformations of the peptides. In this paper, we report the first determination of the gas-phase acidities of the thiol group in two cysteine-polyalanine peptides, $HSCA_3$ and $HSCA_4$. The C-termini are amidated to avoid the complication by the C-terminal carboxyl group.
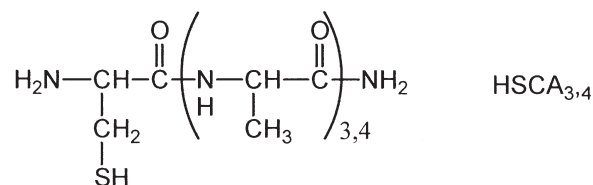
Experimental

The gas-phase acidities ($\Delta_{acid}G$) and the enthalpies of deprotonation ($\Delta_{acid}H$) of the peptides $HSCA_{3,4}$ were determined by using the extended Cooks' kinetic method in which entropy effects were taken into consideration [5–9]. The validity and limitations of using the extended kinetic method to determine thermochemical quantities have been thoroughly discussed in

current literature [10–14]. Briefly, a series of proton-bound dimers ($[A \cdot H \cdot A_i]^-$) of deprotonated $HSCA_{3,4}$ (HA) with a set of conjugate bases of reference acids (HA_i) were generated in the ESI source of the mass spectrometer. The reference acids all have known gas-phase acidities. Each proton-bound dimer was activated by collisions with argon atoms and underwent competitive unimolecular dissociations (the CID process) to produce two ionic products, A^- and A_i^-, with rate constants of k and k_i, respectively, Scheme **1**.

With the assumption that there are no reverse activation barriers for either dissociation channel, the natural logarithm of the ratio of the rate constants has a linear correlation to the difference in the gas-phase acidities, eq 1, where R is the gas constant, T_{eff} is the effective temperature of the activated dimer ion, and $\Delta_{acid}H$ and $\Delta_{acid}H_i$ are the gas-phase enthalpies of deprotonation of HA and the reference acid, respectively. The effective temperature is an empirical parameter that depends on several experimental variables and properties of the proton-bound dimers [15–20]. The term $\Delta(\Delta S)$ is the difference of the activation entropies between the two competing dissociation channels, $\Delta S^{\neq}$(with k) - $\Delta S^{\neq}$(with k_i). The ratio of the rate constants (k/k_i) can be assumed to be equal to the CID product ion branching ratios ($[A^-]/[A_i^-]$), if secondary fragmentation is negligible. To have a proper statistical treatment of the uncertainty through the data analysis, the average gas-phase acidity of the reference acids, $\Delta_{acid}H_{avg}$, introduced in eq 1 was converted to eq 2, where $\ln([A^-]/[A_i^-])$ has a linear relationship with $\Delta_{acid}H_i$-$\Delta_{acid}H_{avg}$ [21]. To obtain the value of $\Delta_{acid}H$, the proton-bound dimers were activated at several different collision energies and the CID product ion branching ratios were measured at each collision energy. Two sets of thermo-kinetic plots were generated from eq 2. The first set consists of linear plots of $\ln([A^-]/[A_i^-])$ versus $\Delta_{acid}H_i$-$\Delta_{acid}H_{avg}$ with $1/RT_{eff}$ as the slope and $-[(\Delta_{acid}H-\Delta_{acid}H_{avg})/RT_{eff}-\Delta(\Delta S)/R]$ as the intercept. The second set is the plot of $[(\Delta_{acid}H-\Delta_{acid}H_{avg})/RT_{eff}-\Delta(\Delta S)/R]$ obtained from the first set against $1/RT_{eff}$ to generate a Van't Hoff-like plot with a slope of $\Delta_{acid}H-\Delta_{acid}H_{avg}$ and an intercept of $-\Delta(\Delta S)/R$. Combination of $\Delta_{acid}H$ and the entropy term, $T\Delta(\Delta S)$, gives the apparent gas-phase acidity of the acid HA, eq 3. The uncertainty was determined based on the error analysis using the ODRFIT program developed by Ervin and Armentrout [10]. This program incorporates the ODRPACK [22] and Monte Carlo simulations for error analysis. An advantage of this program is that it takes into all of the data simultaneously avoiding intermediate linear regressions and the second set of thermo-kinetic plots that could introduce false correlations.

$$\ln\left(\frac{k}{k_i}\right) = \frac{\Delta_{acid}H_i}{RT_{eff}} - \left[\frac{\Delta_{acid}H}{RT_{eff}} - \frac{\Delta(\Delta S)}{R}\right] \tag{1}$$

$$\ln\left(\frac{[A^-]}{[A_i^-]}\right) = \frac{\Delta_{acid}H_i - \Delta_{acid}H_{avg}}{RT_{eff}}$$
$$- \left[\frac{\Delta_{acid}H - \Delta_{acid}H_{avg}}{RT_{eff}} - \frac{\Delta(\Delta S)}{R}\right] \tag{2}$$

$$\Delta_{acid}G^{app} = \Delta_{acid}H - T\Delta(\Delta S) \tag{3}$$

The experiments were carried out using a triple quadrupole mass spectrometer (Varian 1200L, Walnut Creek, CA) located in the Mass Spectrometry Center of the Chemistry Department at the University of the Pacific. The instrument consists of a near-horizontal ESI source with the nitrogen drying gas flowing through a capillary, a hexapole ion guide at a pressure of about 1 mTorr, and a triple quadrupole mass analyzer with a curved collision chamber. Ions generated in the ESI source are presumably thermalized by multiple collisions with the bath gas molecules in the ion guide chamber. The voltage of the ESI needle was set at -4.5 kV and the drying gas temperature was set at 150 °C. The first important step to carry out the acidity measurements was to generate stable proton-bound dimer ions. Each proton-bound dimer ion was formed by infusion of a solution of methanol and water (50:50, vol/vol) containing a mixture of a reference acid and a peptide (10^{-5}-10^{-4} M) into the ESI (negative mode) chamber at a flow rate of 10 μL/min. The signal of the dimer was optimized by adjusting the instrumental conditions, especially the capillary voltage. The dimer ion was isolated with the first quadrupole and was subjected to CID experiments in the collision chamber with argon as the collision gas (0.50 ± 0.03 mTorr). The dissociation product ions were analyzed by the third quadrupole. To examine possible secondary fragmentations, a CID spectrum with a wider range of m/z values was recorded for each proton-bound dimer at several collision energies and the observed secondary fragments were taken into consideration in the data analysis. The CID product ion intensities were measured by setting the instrument in a single reaction monitoring (SRM) mode in which the scan was focused on selected product ions. Multiple measurements were performed on different days and the results were repeatable with a relative uncertainty within $\pm 5\%$. For each proton-bound dimer, the CID experiment was carried out at several collision energies between 0.5 and 2.5 eV in the center-of-mass frame (E_{cm}). The center-of-mass energy was calculated using the equation: $E_{cm} = E_{lab}[m/(M + m)]$, where E_{lab} is the collision energy in laboratory frame, m is the mass of argon and M is the mass of the proton-bound dimer ion.

The peptides were synthesized in our laboratory using the standard method of solid-phase peptide synthesis [23]. The apparatus consists of glass peptide

$$AH + A_i^- \xleftarrow{\ k_i\ } [A \bullet H \bullet A_i]^- \xrightarrow{\ k\ } A^- + HA_i$$

Scheme 1

Table 1. The thermochemical quantities of the reference acids used in this research

Reference acid	$\Delta_{acid}H$, expt[a] (kcal/mol)	$\Delta_{acid}G$, expt[a] (kcal/mol)
F_2CHCO_2H	331.0 ± 2.2	323.8 ± 2.0
$Cl_2CHCO2H$	328.4 ± 2.1	321.9 ± 2.0
$Br_2CHCO2H$	328.3 ± 2.2	321.3 ± 2.0
F_3CCO2H	323.8 ± 2.9	317.4 ± 2.0
$C_3F_7CO_2H$	321.9 ± 2.2	314.9 ± 2.0

[a]Obtained from the NIST Chemistry Webbook [27].

synthesis vessels (Kemtech America, Inc., Whittier, CA) mounted on an agitator assembled in our laboratory. The aminomethyl Rink amide resin (Sigma-Aldrich Co., Milwaukee, WI) was used as the solid support to yield the amide C-terminus. All chemicals used in peptide synthesis, including fmoc-cysteine and fmoc-alanine, were purchased from Sigma-Aldrich Chemical Co. and were used without further purification.

Results and Discussion

Five structurally similar halogenated carboxylic acids (HA_i) with known gas-phase acidities were selected as the references: F_2CHCO_2H, Cl_2CHCO_2H, Br_2CHCO_2H, F_3CCO_2H, and $CF_3CF_2CF_2CO_2H$ ($C_3F_7CO_2H$), Table 1. We first examined the relative acidities of the peptides, $HSCA_{3,4}$, by using the CID-bracketing experiments. The proton-bound dimers of $[A_i \cdot H \cdot SCA_{3,4}]^-$ were generated by ESI. The CID experiments were performed at 1.2 eV (E_{cm}) collision energy and the CID spectra were recorded. The ion intensity of SCA_3^- is slightly stronger than that of $Cl_2CHCO_2^-$ and weaker than that of $Br_2CHCO_2^-$, suggesting that the acidity of $HSCA_3$ is comparable to those of these two reference acids. The ion intensity of $HSCA_4^-$ is about twice as strong as that of $Br_2CHCO_2^-$ and about half of that of $F_3CCO_2^-$, suggesting that $HSCA_4$ has an acidity between those of Br_2CHCO_2H and F_3CCO_2H.

We determined the gas-phase acidities of $HSCA_{3,4}$ using the extended kinetic method. The intensities of all CID product ions were measured at three collision energies: 1.0, 1.5 and 2.0 eV (E_{cm}). At a lower energy (0.5 eV), some CID product ion signals were too weak to produce repeatable data. At a higher energy (2.5 eV), some proton-bound dimers yielded significant second-

ary CID fragment ions. There are three isotopic peaks for the dimers with Cl_2CHCO_2H and Br_2CHCO_2H. The most abundant isotopic peaks were selected as the precursor ions for the CID experiments. About 5% of $SCA_{3,4}^-$ fragmented further by losing H_2S at 2 eV. The proton-bound dimers with $C_3F_7CO_2H$ yielded significant secondary fragments from $C_3F_7CO_2^-$ by losing the CO_2 group. All secondary fragments were included in the data analysis. The CID product ion branching ratios ($[A^-]/[A_i^-]$) measured at the three energies are shown in Table 2. The natural logarithms of the branching ratios from all five proton-bound dimers were used to construct the first set of the thermo-kinetic plots for the $HSCA_3$ system. All proton-bound dimers, except the one with F_2CHCO_2H as the reference acid, were used for the $HSCA_4$ system. The plots of $ln([SCA_3^-]/[A_i^-])$ and $ln([SCA_4^-]/[A_i^-])$ against $\Delta_{acid}H_i-\Delta_{acid}H_{avg}$ are shown in Figures 1a and 2a, where $\Delta_{acid}H_{avg}$ is 326.7 ± 1.8 kcal/mol for the $HSCA_3$ system and 325.6 ± 1.8 kcal/mol for the $HSCA_4$ system. The uncertainty of the average acidity was calculated as the root sum square of the random and systematic errors. The random error was treated as the averaged uncertainty of the reference acids (± 2.3) divided by the square root of the number of the reference acids, $(2.3/\sqrt{5}) = 1.0$ kcal/mol, and the systematic error was assigned as $\sqrt{2.3} = 1.5$ kcal/mol. The root sum square of the random and systematic errors yielded $\sqrt{(1.0^2 + 1.5^2} = 1.8$ kcal/mol. Linear regression with the least-squares fit of the data points measured at each collision energy gives a straight line with the slope of $1/RT_{eff}$ and the y-intercept of $-[(\Delta_{acid}H-\Delta_{acid}H_{avg})/RT_{eff}-\Delta(\Delta S)/R]$. The resulting slopes and intercepts along with the derived effective temperatures are summarized in Table 3. The $HSCA_3$ system has relatively smaller uncertainties than those of the $HSCA_4$ system. The data were further analyzed by weighted orthogonal distance regression (ODR) using the ODRPACK suite of programs [22] and the results were essentially the same as those obtained from the least-squares analysis. The x-intercepts of the best-fit lines indicate the apparent gas-phase acidities. The values are in the ranges of 320.9 to 322.2 kcal/mol for $HSCA_3$ and 319.0 to 320.2 kcal/mol for $HSCA_4$. For both systems, the extrapolated linear plots crossed at a single point that represents the temperature-independent isothermal point for the system [13]. The isothermal point has negative x- and y-values, indicating that the en-

Table 2. CID product ion ratios ($[SCA_{3,4}^-]/[A_i^-]$) from the dissociation of $[A_i \bullet H \bullet SCA_{3,4}]^-$ at three collision energies, E_{cm} (with $\pm 5\%$ of uncertainty)

HA$_i$	HSCA$_3$			HSCA$_4$		
	1.0 eV	1.5 eV	2.0 eV	1.0 eV	1.5 eV	2.0 eV
F_2CHCO_2H	15.2	6.52	4.26	(95.0)	(42.6)	(33.2)
Cl_2CHCO_2H	1.46	0.796	0.542	9.22	4.56	3.01
Br_2CHCO_2H	1.05	0.660	0.480	5.11	2.81	1.79
F_3CCO_2H	0.0702	0.0464	0.0382	0.416	0.306	0.252
$C_3F_7CO_2H$	0.00802	0.00609	0.00539	0.0330	0.0255	0.0192

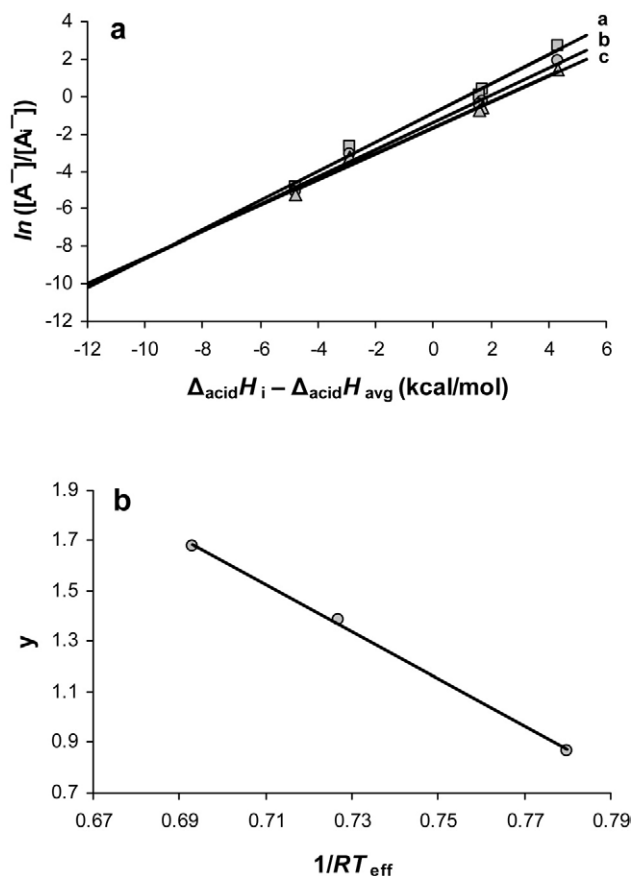**Figure 1.** (a) Plots of $\ln([A^-]/[A_i^-])$ versus $\Delta_{acid}H_i$-$\Delta_{acid}H_{avg}$ from the dissociation of $[A_i \cdot H \cdot SCA_3]^-$ at three collision energies, E_{cm}: 1.0 eV, $R^2 = 0.987$ (**a**); 1.5 eV, $R^2 = 0.990$ (**b**); and 2.0 eV, $R^2 = 0.989$ (**c**). (b) Plot of $y = (\Delta_{acid}H$-$\Delta_{acid}H_{avg})/RT_{eff}$-$\Delta(\Delta S)/R$ versus $1/RT_{eff}$, $y = -9.39x + 8.19$, $R^2 = 0.999$.

thalpy of deprotonation is smaller than the apparent gas-phase acidity.

The enthalpies of deprotonation for $HSCA_{3,4}$ were derived from the second set of the thermo-kinetic plots. The plot was generated by plotting the values of $[(\Delta_{acid}H$-$\Delta_{acid}H_{avg})/RT_{eff}$-$\Delta(\Delta S)/R]$ obtained from the first set of the plots against the corresponding $1/RT_{eff}$, Figures 1b and 2b. Linear regression with least-squares fit of each set of the data gives a straight line with a slope of $\Delta_{acid}H$-$\Delta_{acid}H_{avg}$ and an intercept of -$\Delta(\Delta S)/R$. The slope and the intercept correspond to the x- and the y-values at the isothermal points in Figures 1a and 2a. The data were further analyzed using the ODRPACK program. The two data-fitting methods give essentially the same results. The slopes and the intercepts obtained are -9.39 ± 0.33 and 8.19 ± 0.24 for the $HSCA_3$ system, and -9.39 ± 0.85 and 6.53 ± 0.62 for the $HSCA_4$ system, respectively. Combining the slopes with the corresponding values of $\Delta_{acid}H_{avg}$, we obtained $\Delta_{acid}H(HSCA_3)$ to be 317.3 ± 2.0 kcal/mol and $\Delta_{acid}H(HSCA_4)$ to be 316.2 ± 2.0 kcal/mol.

In a separate experiment, we included F_2CHCO_2H as a reference for the $HSCA_4$ system. In this case, the derived value of $\Delta_{acid}H(HSCA_4)$ was lower by 0.5

kcal/mol and the uncertainty was much larger, ± 3.2 kcal/mol. One indication of the larger uncertainty is that the extrapolated linear plots in the first set of the thermo-kinetic plots did not converge to a single point. The reason will be discussed in a later section of the paper.

The intercepts of the second set of the linear plots give the values of $\Delta(\Delta S)$ to be -16.3 ± 0.2 cal/mol K for the $HSCA_3$ system and -13.0 ± 1.2 cal/mol K for the $HSCA_4$ system. At 298 K, the entropy terms would contribute 4.8 and 3.9 kcal/mol to the apparent gas-phase acidities of $HSCA_3$ and $HSCA_4$, respectively. Using the thermochemical relationship shown in eq 3, we obtained the apparent gas-phase acidities, $\Delta_{acid}G^{app}$, of $HSCA_3$ to be 322.1 ± 2.0 kcal/mol and of $HSCA_4$ to be 320.1 ± 2.0 kcal/mol (Table 4). The apparent acidities agree well with the observations in the CID bracketing experiments. The apparent acidity of $HSCA_3$ is comparable to the acidity of Cl_2CHCO_2H ($\Delta_{acid}G = 321.9 \pm 2.0$ kcal/mol) and the apparent acidity of $HSCA_4$ is slightly lower than the acidity of Br_2CHCO_2H ($\Delta_{acid}G = 321.3 \pm 2.0$ kcal/mol).
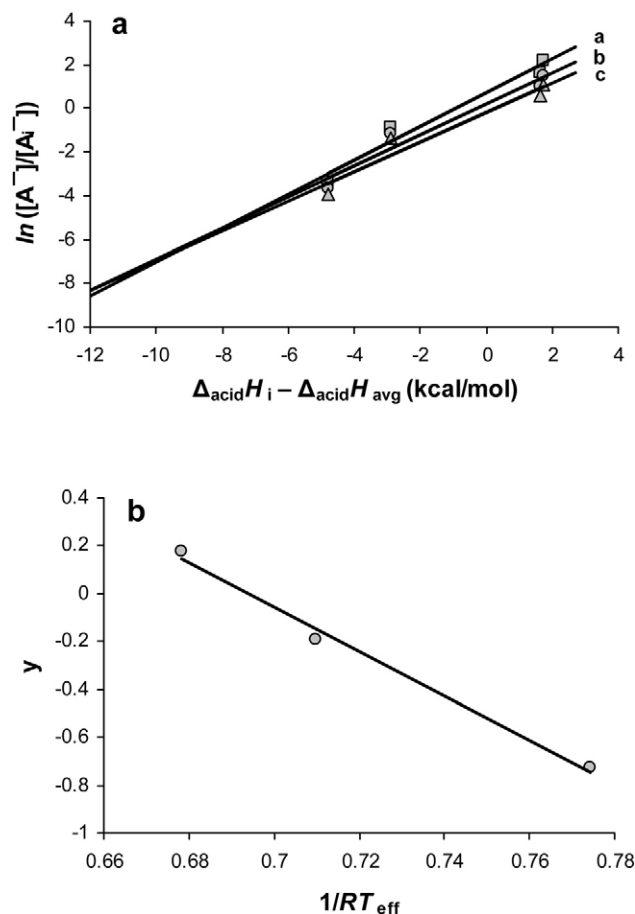

Figure 2. (a) Plots of $\ln([A^-]/[A_i^-])$ versus $\Delta_{acid}H_i$-$\Delta_{acid}H_{avg}$ from the dissociation of $[A_i \cdot H \cdot SCA_4]^-$ at three collision energies, E_{cm}: 1.0 eV, $R^2 = 0.963$ (**a**); 1.5 eV, $R^2 = 0.954$ (**b**); and 2.0 eV, $R^2 = 0.938$ (**c**). (b) Plot of $y = (\Delta_{acid}H$-$\Delta_{acid}H_{avg})/RT_{eff}$-$\Delta(\Delta S)/R$ versus $1/RT_{eff}$, $y = -9.39x + 6.53$, $R^2 = 0.992$.

Table 3. Results obtained from the linear regression of the experimental data according to eq 2, where the uncertainties refer to 95% conference level

	HSCA$_3$			HSCA$_4$		
E_{cm}, eV	$1/RT_{eff}$	$-[(\Delta_{acid}H - \Delta_{acid}H_{avg})/RT_{eff} - \Delta(\Delta S)/R]$	T_{eff}, K	$1/RT_{eff}$	$-[(\Delta_{acid}H - \Delta_{acid}H_{avg})/RT_{eff} - \Delta(\Delta S)/R]$	T_{eff}, K
1.0	0.780 ± 0.051	−0.868 ± 0.171	645 ± 39	0.774 ± 0.106	0.728 ± 0.234	585 ± 58
1.5	0.727 ± 0.041	−1.388 ± 0.139	692 ± 41	0.709 ± 0.109	0.190 ± 0.332	650 ± 65
2.0	0.693 ± 0.041	−1.677 ± 0.138	726 ± 44	0.678 ± 0.123	−0.179 ± 0.374	709 ± 70

We evaluated the results obtained from the extended kinetic method by fitting the experimental data using the ODRFIT program [10]. Full entropy analysis with 10,000 iterations in Monte Carlo simulations yielded the enthalpy of deprotonation for the two peptides to be $\Delta_{acid}H$(HSCA$_3$) = 317.5 ± 2.4 kcal/mol and $\Delta_{acid}H$(HSCA$_4$) = 315.5 ± 3.9 kcal/mol. The entropy terms, $\Delta(\Delta S)$, were derived to be −16.1 ± 3.1 cal/mol K for the HSCA$_3$ system and −16.3 ± 5.6 cal/mol K for the HSCA$_4$ system. These results are listed in Table 4. The results obtained from the ODRFIT program show larger uncertainties and the absolute values are in reasonably good agreements with those derived from the two sets of thermo-kinetic plots. Considering the large entropy effects involved in these systems, we assign the errors obtained from ODRFIT program as the uncertainty for the final values of the enthalpies of deprotonation and the acidities.

The enthalpies of deprotonation (at the isothermal point) of HSCA$_3$ ($\Delta_{acid}H$ = 317.3 ± 2.4 kcal/mol) and HSCA$_4$ ($\Delta_{acid}H$ = 316.2 ± 3.9 kcal/mol) are significantly lower (4 to 5 kcal/mol) than the apparent gas-phase acidities ($\Delta_{acid}G$(HSCA$_3$) = 322.1 ± 2.4 kcal/mol and $\Delta_{acid}G$(HSCA$_4$) = 320.1 ± 3.9 kcal/mol). The differences come from the entropy contribution upon fragmentation of the proton-bound dimer, [A$_i$·H·SCA$_{3,4}$ [6, 24]. The term $\Delta(\Delta S)$ corresponds to the difference in activation entropies, $\Delta S^{\neq}$(channel k) minus $\Delta S^{\neq}$(channel ki), Scheme 1. In both HSCA$_{3,4}$ systems, the values of $\Delta(\Delta S)$ are negative, suggesting that the dissociation channel leading to the formation of the deprotonated peptides is entropically less favored than that leading to the formation of the deprotonated reference acids.

The entropy effects on the observed CID product ion branching ratios can be examined by plotting the logarithms of the branching ratios as a function of the collision energy. For each proton-bound dimer, we measured the branching ratios at five energies, E_{cm} =

0.5, 1.0, 1.5, 2.0, and 2.5 eV. The plots of ln([SCA$_{3,4}^-$]/[A$_i^-$]) against E_{cm} are given in Figures 3 and 4. Both systems show similar trends that the values of ln([SCA$_{3,4}^-$]/[A$_i^-$]) decrease nearly parallel as the collision energy is increased, except for the plot of ln([SCA$_4^-$]/[F$_2$CHCO$_2^-$]), which curves up at about 2.0 eV (Figure 4). In Figure 3, the plots with A$_i^-$ = Cl$_2$CHCO$_2^-$ and Br$_2$CHCO$_2^-$ cross the "zero" line, where ln([A$^-$]/[A$_i^-$]) = 0, at about 1.0 to 1.3 eV, and in the HSCA$_4$ system, the plot with F$_3$CCO$_2^-$ has a tendency to cross the "zero" line below 0.5 eV. These behaviors strongly suggest that the absolute values of $\Delta(\Delta S)$ are significantly larger than zero. The parallel pattern indicates that the values of $\Delta(\Delta S)$ are about the same for all of the proton-bound dimers involved in each system [6]. The plots would approach to the "zero" line from both the positive and the negative directions as the collision energy is increased, if the entropy term were negligible. This can be qualitatively understood by examining each term in eq 1. The T_{eff} is related to the collision energy. As the collision energy is increased, the T_{eff} becomes higher, and the absolute value of the term $\Delta_{acid}H_i/RT_{eff}$-$\Delta_{acid}H/RT_{eff}$ becomes smaller. If $\Delta(\Delta S)$ is negligible, then the value of $ln(k/k_i)$ would approach zero as T_{eff} is increased. If $\Delta(\Delta S)$ is a significant and constant value, then the difference between a pair of $ln(k/k_i)$ would be $\Delta(\Delta S)/R$ at each T_{eff}. If $\Delta(\Delta S)$ is negative, then all plots of $ln(k/k_i)$ would be parallel and pointing towards the negative direction. The fact that the plot with F$_2$CHCO$_2$H as the reference acid for the HSCA$_4$ system is curving up indicates that the entropy term for the dissociation of [F$_2$CHCO$_2$·H·SCA$_4$]$^-$ may change from negative to positive at higher collision energy. The change in activation entropy implies a large conformation change of the proton-bound dimer upon dissociation [6, 24]. This might be the reason for the large uncertainty of the resulting gas-phase acidity when F$_2$CHCO$_2$H was used as the reference acid for

Table 4. Results obtained from the second set of thermo-kinetic plots of EKM^a and the ODRFIT program, where $\Delta_{acid}G^{app}$ is calculated according to eq 3

Peptide	$\Delta_{acid}H$ (kcal/mol) EKM	$\Delta(\Delta S)$ (cal/mol K) EKM	$\Delta_{acid}G^{app}$ (kcal/mol) EKM	$\Delta_{acid}H$ (kcal/mol) ODRFIT	$\Delta(\Delta S)$ (cal/mol K) ODRFIT
HSCA$_3$	317.3 ± 2.0	−16.3 ± 0.2	322.1 ± 2.0	317.5 ± 2.4	−16.1 ± 3.1
HSCA$_4$	316.2 ± 2.0	−13.0 ± 1.2	320.1 ± 2.0	315.5 ± 3.9	−16.2 ± 5.6

^{a}EKM: Extended kinetic method.

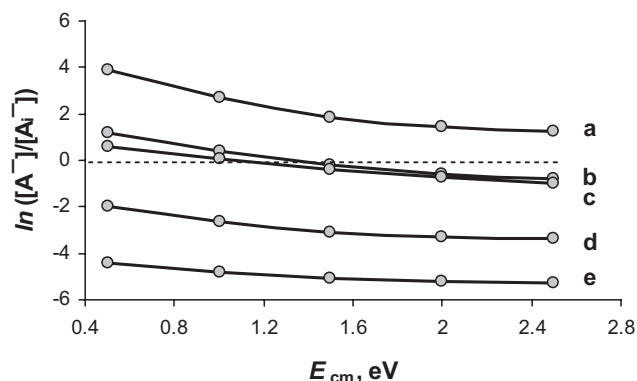**Figure 3.** Plots of $\ln([A^-]/[A_i^-])$ versus E_{cm} from the dissociation of $[A_i \cdot H \cdot SCA_3]^-$, where A_i^- is $F_2CHCO_2^-$ (**a**), $Cl_2CHCO_2^-$ (**b**), $Br_2CHCO_2^-$ (**c**), $F_3CCO_2^-$ (**d**), and $C_3F_7CO_2^-$ (**e**).

HSCA$_4$. We are examining the conformations associated with the dissociation process computationally, and the results will be published in a later article.

The entropy effects can also be viewed through the examination of the dissociation dynamics of the proton-bound dimers. The activation entropy corresponds to the density of states at the transition-state. A relatively large positive entropy indicates a "loose" transition-state compared with a "tight" transition-state. Figure 5 shows a schematic drawing of the potential energy surface for the dissociation of $[Cl_2CHCO_2 \cdot H \cdot SCA_3]^-$. Channel **A** has a relatively lower activation energy and a tighter transition-state compared with channel **B**. As the collision energy is increased, the internal energy of the dimer ion becomes higher and the dissociation rate constants for both channels become larger. Since channel **A** has a tighter transition-state, the degree of increment in the rate constant is smaller than that of channel **B**. As a consequence the logarithm of the branching ratio, $\ln(k/k_i) \approx \ln([SCA_3^-]/[Cl_2CHCO_2^-])$, decreases as a function of increase in collision energy, changing from a positive value to a negative one at about 1.3 eV. The tighter transition-state in channel **A** is likely due to the formation of SCA_3^- with a relatively rigid conformation.
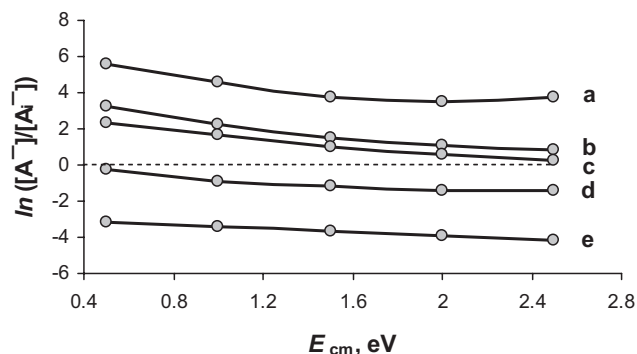

Figure 4. Plots of $\ln([A^-]/[A_i^-])$ versus E_{cm} from the dissociation of $[A_i \cdot H \cdot SCA_4]^-$, where A_i^- is $F_2CHCO_2^-$ (**a**), $Cl_2CHCO_2^-$ (**b**), $Br_2CHCO_2^-$ (**c**), $F_3CCO_2^-$ (**d**), and $C_3F_7CO_2^-$ (**e**).
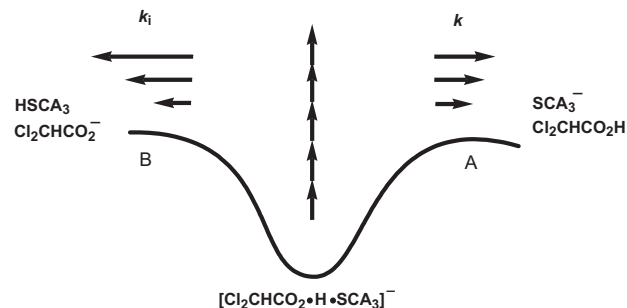

Figure 5. A schematic drawing of the potential energy surface for the dissociation of $[Cl_2CHCO_2 \cdot H \cdot SCA_3]^-$.

To examine the effect of the peptide chain on the acidity of the thiol group in HSCA$_{3,4}$, we calculated the theoretical acidity of the amidated-cysteine (HSC), $HSCH_2C(NH_2)CONH_2$, using density functional theory at the B3LYP/6-31 + G(d) level [25]. The calculations were performed using the Gaussian 03W computational program [26]. The gas-phase enthalpy of deprotonation of HSC was calculated to be $\Delta_{acid}H$ = 338 kcal/mol using the isodesmic proton transfer reaction, HSC + $SCH_2CH_3^- \rightarrow SC^-$ + $HSCH_2CH_3$. Compared with HSC, the acidity of the thiol group in HSCA$_{3,4}$ is stronger by about 20 kcal/mol. The increased acidity is likely due to the stabilization of the negatively charged thiolate group by the peptide chain through internal solvation.

Conclusions

We determined the gas-phase deprotonation enthalpies of two cysteine-polyalanine peptides, HSCA$_{3,4}$, using the extended kinetic method with full entropy analysis. The values obtained are $\Delta_{acid}H(HSCA_3)$ = 317.3 ± 2.4 kcal/mol and $\Delta_{acid}H(HSCA_4)$ = 316.2 ± 3.9 kcal/mol. In these systems, the entropy term is significant and has large effects (4 to 5 kcal/mol) on the apparent acidities. The corresponding apparent gas-phase acidities, $\Delta_{acid}G^{app}$, were derived to be 322.1 ± 2.4 kcal/mol (HSCA$_3$) and 320.1 ± 3.9 kcal/mol (HSCA$_4$), respectively. The derived apparent acidities are in good agreement with the results obtained from the CID bracketing experiments. Compared with that in the isolated cysteine residue, the thiol group in these cysteine-polyalanine peptides has a stronger gas-phase acidity by about 20 kcal/mol. The increased acidity is likely due to the stabilization of the negatively charged thiolate group by the peptide chain through internal solvation upon deprotonation.

Acknowledgments

References

1. Raina, S.; Missiakas, D. Making and Breaking Disulfide Bonds. *Annu. Rev. Microbiol.* **1997,** *51,* 179–202.
2. Kortemme, T.; Darby, N. J.; Creighton, T. E. Electrostatic Interactions in the Active Site of the N-Terminal Thioredoxin-Like Domain of Protein Disulfide Isomerase. *Biochemistry* **1996,** *35,* 14503–14511.
3. Takahashi, N.; Creighton, T. E. On the Reactivity and Ionization of the Active Site Cysteine Residues of Escherichia coli Thioredoxin. *Biochemistry* **1996,** *35,* 8342–8353.
4. Kortemme, T.; Creighton, T. E. Ionization of Cysteine Residues at the Termini of Model A-Helical Peptides. Relevance to Unusual Thiol pKa Values in Proteins of the Thioredoxin Family. *J. Mol. Biol.* **1995,** *253,* 799–812.
5. Cooks, R. G.; Patrick, J. S.; Kotiaho, T.; McLuckey, S. A. Thermochemical Determinations by the Kinetic Method. *Mass Spectrom. Rev.* **1994,** *13,* 287–339.
6. Cheng, X.; Wu, Z.; Fenselau, C. Collision Energy Dependence of Proton-Bound Dimer Dissociation: Entropy Effects, Proton Affinities, and Intramolecular Hydrogen-Bonding in Protonated Peptides. *J. Am. Chem. Soc.* **1993,** *115,* 4844–4848.
7. Cerda, B. A.; Wesdemiotis, C. Li+, Na+, and K+ Binding to the DNA and RNA Nucleobases. Bond Energies and Attachment Sites from the Dissociation of Metal Ion-Bound Heterodimers. *J. Am. Chem. Soc.* **1996,** *118,* 11884–11892.
8. Cooks, R. G.; Wong, P. S. H. Kinetic Method of Making Thermochemical Determinations: Advances and Applications. *Acc. Chem. Res.* **1998,** *31,* 379–386.
9. Williams, T. I.; Denault, J. W.; Cooks, R. G. Proton Affinity of Deuterated Acetonitrile Estimated by the Kinetic Method with Full Entropy Analysis. *Int. J. Mass Spectrom.* **2001,** *210/211,* 133–146.
10. Ervin, K. M.; Armentrout, P. B. Systematic and Random Errors in Ion Affinities and Activation Entropies from the Extended Kinetic Method. *J. Mass Spectrom.* **2004,** *39,* 1004–1015.
11. Drahos, L.; Peltz, C.; Vekey, K. Accuracy of Enthalpy and Entropy Determination Using the Kinetic Method: Are We Approaching a Consensus? *J. Mass Spectrom.* **2004,** *39,* 1016–1024.
12. Bouchoux, G. Microcanonical Modeling of the Thermokinetic Method. *J. Phys. Chem. A* **2006,** *110,* 8259–8265.
13. Bouchoux, G.; Sablier, M.; Berruyer-Penaud, F. Obtaining Thermochemical Data by the Extended Kinetic Method. *J. Mass Spectrom.* **2004,** *39,* 986–997.
14. Wesdemiotis, C. Entropy Considerations in Kinetic Method Experiments. *J. Mass Spectrom.* **2004,** *39,* 998–1003.
15. Drahos, L.; Vekey, K. How Closely Related are the Effective and the Real Temperature. *J. Mass Spectrom.* **1999,** *34,* 79–84.
16. Armentrout, P.B. Is the Kinetic Method a Thermodynamic Method? *J. Mass Spectrom.* **1999,** *34,* 74–78.
17. Laskin, J.; Futrell, J. H. The Theoretical Basis of the Kinetic Method from the Point of View of Finite Heat Bath Theory. *J. Phys. Chem. A* **2000,** *104,* 8829–8837.
18. Ervin, K. M. Microcanonical Analysis of the Kinetic Method. The Meaning of the "Apparent Entropy." *J. Am. Soc. Mass Spectrom.* **2002,** *13,* 435–452.
19. Norrman, K.; McMahon, T. B. Relationship Between Effective Temperature of Thermalized Ions and Ion Source Temperature. *Int. J. Mass Spectrom.* **1998,** *176,* 87–97.
20. Cooks, R. G.; Koskinen, J. T.; Thomas, P. D. The Kinetic Method of Making Thermochemical Determinations. *J. Mass Spectrom.* **1999,** *34,* 85–92.
21. Armentrout, P. B. Entropy Measurements and the Kinetic Method: A Statistically Meaningful Approach. *J. Am. Soc. Mass Spectrom.* **2000,** *11,* 371–379.
22. Boggs,, P. T.; Byrd,, R. H., Rogers,, J. E.; Schnabel,, R. B. ODRPACK Version 2.01 Software for Weighted Orthogonal Distance Regression. *Report NISTIR 92-4834*; National Institute of Standards and Technology: Gaithersburg, MD, 1992.
23. Gutte, B., Ed. *Peptides: Synthesis, Structures, and Applications*; San Diego, CA: Academic Press, 1995, pp 94-159.
24. Hahn, I. S.; Wesdemiotis, C. Protonation Thermochemistry of β-Alanine an Evaluation of Proton Affinities and Entropies Determined by the Extended Kinetic Method. *Int. J. Mass Spectrom.* **2003,** *222,* 465–479.
25. Becke, A. D. Density-functional thermochemistry. III. The Role of Exact Exchange. *J. Chem. Phys.* **1993,** *98,* 5648–5652.
26. Frisch, M. J.; Trucks, G. W.; Schlegel, H. B.; Scuseria, G. E.; Robb, M. A.; Cheeseman, J. R.; J.A. Montgomery, J.; Vreven, T.; Kudin, K. N.; Burant, J. C.; Millam, J. M.; Iyengar, S. S.; Tomasi, J.; Barone, V.; Mennucci, B.; Cossi, M.; Scalmani, G.; Rega, N.; Petersson, G. A.; Nakatsuji, G.; Hada, M.; Ehara, M.; Toyota, K.; Fukuda, R.; Hasegawa, J.; Ishida, M.; Nakajima, T.; Honda, Y.; Kitao, O.; Nakai, H.; Klene, M.; Li, X.; Knox, J. E.; Hratchian, H. P.; Cross, J. B.; Adamo, C.; Jaramillo, J.; Gomperts, R.; Stratmann, R. E.; Yazyev, O.; Austin, A. J.; Cammi, R.; Adamo, C.; Jaramillo, J.; Gomperts, R.; Stratmann, R. E.; Yazyev, O.; Austin, A. J.; Cammi, R.; Pomelli, C.; Ochterski, J. W.; Ayala, P. Y.; Morokuma, K.; Voth, G. A.; Salvador, P.; Dannenberg, J. J.; Zakrzewski, V. G.; Dapprich, S.; Daniels, A. D.; Strain, M. C.; Farkas, O.; Malick, D. K.; Rabuck, A. D.; Raghavachari, K.; Foresman, J. B.; Ortiz, J. V.; Cui, Q.; Baboul, A. G.; Cliford, S.; Cioslowski, J.; Stefanov, B. B.; Liu, G.; Liashenko, A.; Piskorz, P.; Komaromi, I.; Martin, R. L.; Fox, D. J.; Keith, T.; Al-Laham, M. A.; Peng, C. Y.; Nanayakkara, A.; Challacombe, M.; Gill, P. M. W.; Johnson, B.; Chen, W.; Wong, M. W.; Gonzalez, C.; Pople, J. A. G*aussian 03, Revision A.1*; Gaussian, Inc., Pittsburgh PA, 2003.
27. Linstrom, P. J.; Mallard, W. G., Eds., *NIST Chemistry Webbook, NIST Standard Reference Database Number 69, June 2005 Release*; National Institute of Standards and Technology, Gaithersburg MD, 20899 (http://webbook.nist.gov).